Hierarchical nanostructured porous titania films supported on glass substrate with enhanced photocatalytic efficiency

NITIPONG SANGKHARAT, TANAPOL CHALERMKITI, PORNSIT LORKIT, BUSSARIN KSAPABUTR*, MANOP PANAPOY*
Department of Materials Science and Engineering, Faculty of Engineering and Industrial Technology, Silpakorn University, Sanamchandra Palace Campus, Nakhon Pathom 73000, Thailand

Hierarchical nanostructured porous titania (TiO_2) films supported on glass substrates were directly prepared by electrostatic spray deposition process. This synthesis method is versatile for tailoring TiO_2 nanostructured design from three-dimensional (3D) rods to drops using flat-shaped tip (0°) and wedge-shaped tip (15°), respectively. The photocatalytic efficiency of the catalysts was evaluated by degradation of methylene blue (MB) as a model molecule under ultraviolet irradiation. The resulting films exhibited very promising photocatalytic properties for MB degradation, even superior to P25 film obtained from commercial Degussa powder and showed the catalyst stability and reusability, even after five reuse cycles. The reported strategy also provides a simple technique to fabricate 3D nanostructured films.

(Received November 21, 2015; accepted April 5, 2016)

Keywords: Titanium dioxide, Electrostatic spray deposition, Film, Photocatalyst

1. Introduction

Nanostructured materials with controlled structures and shapes have attracted much attention in both scientific research and practical applications [1–2]. Among various semiconductors, titanium dioxide (titania, TiO_2) has been known as an important functional material owing to its unique characteristics in surface structure, band position, electronic and optical properties, as well as its chemical stability, low cost and non-toxicity [3–4]. However, enhancement of the photocatalytic performance of TiO_2 to meet the practical application requirements is still a challenge because of poor light absorption and rapid recombination of photogenerated electrons and holes caused by its wide band gap responding only to ultraviolet (UV) light [5–6]. Recently, three-dimensional (3D) hierarchical nanostructures have been shown to be one of the most important factors affecting the photocatalytic activity of TiO_2 based photocatalysts, which have superior photocatalytic activity compared with other lower-dimensional nanostructures [7–8]. The hierarchical nanostructures can improve the light absorption of wide band gap semiconductors through the reflection, scattering effect and efficient charge transfer, leading to a superior photocatalytic performance than zero-dimensional (0D) nanostructures [9–11]. However, the use of powder photocatalyst has some drawbacks, especially the requirement for additional steps for stirring during reaction, separating and recovering the photocatalyst after the reaction and the difficulty to handle [10,12]. To overcome these obstacles in using the powder photocatalyst, immobilization of TiO_2 powder on various substrates continues to be an active area of research, but current bottlenecks lie in low photocatalytic activity [13–14]. Thin films of TiO_2 have been produced by different techniques, such as chemical vapor deposition [15], sol–gel [16], impregnation [17], and electrostatic spray deposition (ESD) [10]. Among available deposition processes, ESD technique is a non-vacuum and low-cost deposition method, which allows low-temperature deposition and good control of film composition and morphology. The surface morphology of the films can be controlled by varying the preparation conditions, such as deposition temperature, deposition time, flow rate of precursor solution, distance between nozzle and substrate, and nozzle geometry [18–22].

In this work, we demonstrate the fabrication of 3D hierarchical TiO_2 films on glass substrates without using binders and templates. The effect of nozzle geometry on the atomization of liquid and the film morphology in the ESD process was investigated. The photocatalytic efficiency of the resulting films was evaluated by degradation of methylene blue (MB) in aqueous solution under UV light irradiation. The prepared hierarchical structured films show higher photocatalytic activity than P25 film obtained from commercial Degussa powder.

2. Experimental

2.1 Fabrication of TiO_2 films

TiO_2 coating films on glass substrates were prepared by ESD technique used in previous work [10]. First,

titanium tetraisopropoxide (Acros Organics, 98%) was dissolved in absolute ethyl alcohol (Carlo Erba reagents) to obtain 0.05 M precursor solution. Two different nozzle configurations were investigated: flat-shaped tip (0°) and wedge-shaped tip (15°), as shown in the inset of Fig. 1(a) and 1(b), respectively. The precursor solution was deposited on a glass substrate and kept at a constant temperature of 400 °C using a temperature controller. The deposition time was fixed for 1 h. The flow rate of the precursor solution and electric field were controlled at 1.5 mL/h and 2.5 kV/cm, respectively. After deposition, the as-obtained films were annealed at 600 °C for 2 h to form crystalline TiO_2 films.

2.2 Characterization

The deposition temperature was determined by the thermogravimetric analysis with a Perkin-Elmer TGA 7 thermogravimetric analyser. The TGA result revealed that weight losses occurred below 300 °C corresponding to the evaporation of solvent and isopropanol, and the decomposition of organic residuals. The substrate temperature was therefore kept at 400 °C during deposition. The surface and cross-sectional morphologies of the films were observed using a scanning electron microscope (SEM, Model TM3030, Hitachi). The crystal structure of the samples was analysed using X-ray diffractometer (XRD, Model 6100, Shimadzu). The specific surface area of the samples was measured by nitrogen adsorption with a Quantachrome Autosorb–1–MP instrument. The measurement of electrochemical impedance spectroscopy (EIS) was performed by applying a 50 mV AC signal in the 0.02–100 Hz frequency range using Hioki 3522-50 LCR Hitester. All measurements were carried out in sodium hydroxide (NaOH) solution at pH of 8.

In the photocatalytic testing, about 2 mg of TiO_2 film deposited on glass substrate was immersed in 20 mL of 15 μM MB aqueous solution and kept in the dark condition until the adsorption–desorption equilibrium was reached. The photocatalytic performance of the films was tested by the photocatalytic decolourisation of MB in aqueous solution under UV irradiation (Philips, Hg-Lamp 400 W) at light intensity of 4.0 mW/cm^2. The change in the MB concentration as a function of time was measured using a UV–vis spectrometer (JASCO V–530). Blank test was carried out for MB dye in absence of catalyst under UV light.

3. Results and discussion

Fig. 1 shows the photographs of spray profile during the ESD process using different nozzle geometries and the top-view and cross-sectional SEM images of the resulting films. The rod-like morphology of TiO_2 film was obtained from the nozzle with flat-shaped tip (0°) (Fig. 1(c)). The average rod diameter and length were 164 ± 28 nm and 1832 ± 614 nm, respectively. This is probably because in the case of flat-shaped tip, the precursor solution was emitted along the circumference of orifice outlet in the form of multi-jet spray (Fig. 1(a)), which resulted in a decrease in flow rate of each jet spray and droplet size [23]. The smaller droplet size causes a faster evaporation of organic solvent in the charged droplets and this leads to low spreading of the charged droplets impacting on the substrate, which resulted in the formation of nanorod film. For the wedge-shaped tip (15°), the charge was accumulated at the nozzle tip, as shown in Fig. 1(b) and the charged droplets were ejected from only the nozzle tip, resulting in higher flow rate and larger droplet size compared with those using the flat-shaped tip. The larger droplet size causes a slower solvent evaporation which increases the spreading of charged droplets impacting on the substrate, leading to the formation of TiO_2 film with drop-like morphology (Fig. 1(e)). From the cross-sectional SEM micrographs (Fig. 1(d) and 1(f)), the thickness of the films prepared from flat-shaped tip and wedge-shaped tip was 31.14 ± 2.45 and 43.64 ± 2.26 μm, respectively. This might be because of wider spray angle produced from the use of nozzle with flat-shaped tip, resulting in a thinner film. These results are consistent with previous works for samarium doped ceria films [18].

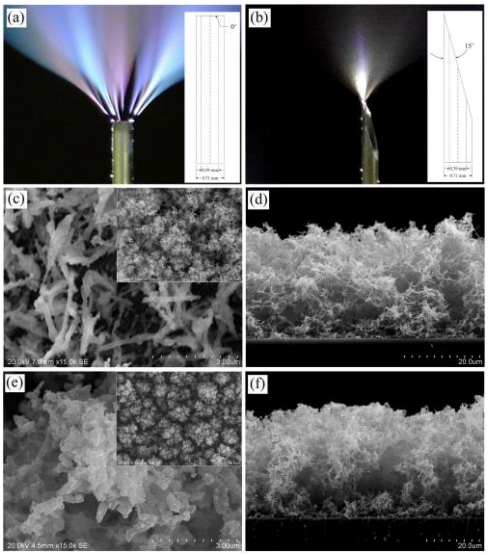

Fig. 1. Photographs of spray profile using (a) flat-shaped tip, (b) wedge-shaped tip (the insets of (a) and (b) show the corresponding schematic drawings of nozzles) and top-view and side-view SEM images of TiO_2 films prepared by (c,d) flat-shaped tip, (e,f) wedge-shaped tip.

The XRD patterns of nanorod and nanodrop TiO_2 films obtained from the flat-shaped tip and wedge-shaped tip, respectively, are demonstrated in Fig. 2. All the diffraction peaks of both films can be indexed to the anatase phase of TiO_2 (JCPDS File no. 21–1272). The average crystallite sizes were determined from the (1 0 1) reflection based on the Scherrer′s equation [24]. The calculated average crystallite size was about 40.9 and 30.4 nm for the nanorod and nanodrop films, respectively. The TiO_2 nanorod film had larger crystallinity and crystallite

size than the TiO_2 nanodrop film because of better heat transfer for lower film thickness [10] for the TiO_2 nanorod film.

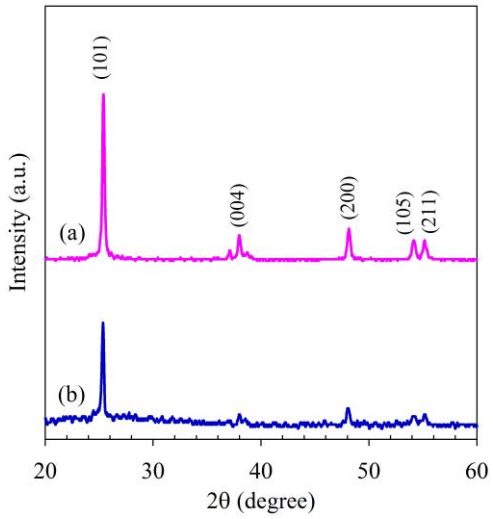

Fig. 2. XRD patterns of TiO_2 films obtained using (a) flat-shaped tip and (b) wedge-shaped tip

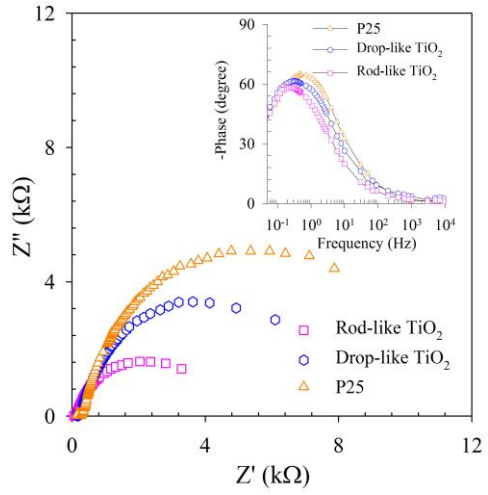

Fig. 3. Nyquist plots obtained for the electrodes in NaOH solution at pH of 8 measured in the frequency range of 0.02 to 100 kHz using AC amplitude of 50 mV (inset: Bodes phase plots)

To study charge separation–transfer and recombination processes, EIS measurement was conducted for the prepared photocatalysts, as well as commercial P25 for comparison under UV irradiation (Fig. 3). The electrochemical impedance spectra of all the samples displays a semicircle. The semicircle with smaller radius suggests the lower charge transfer resistance and the higher separation efficiency for the photogenerated electron–hole pairs [11]. As shown in Fig. 3, the smaller the arc radius, the higher the charge-transfer capability of rod-like TiO_2 film is. The inset in Fig. 3 illustrates the Bode phase plots showing the characteristic frequency peak of the samples. The lifetime (τ_r) of injected electrons can be determined by the position of the low frequency peak in the Bode plots using the equation $\tau_r = 0.5\ (\pi f_{max})^{-1}$, where f_{max} is the frequency at the top of the low frequency arc [11,25]. The characteristic peak of the nanorod film shifted to lower frequency compared with that of other samples. The electron lifetime for nanorod, nanodrop and P25 films was about 0.723, 0.468 and 0.332 s, respectively. The longer electron lifetimes can be ascribed to higher electron mobility in the rod-like film suggesting the decrease in charge recombination rate and the increase in separation of charge carriers.

The photocatalytic efficiency of different photocatalysts was investigated by the decolourisation of MB solution under UV irradiation. Fig. 4 displays the photocatalytic degradation of MB and pseudo-first-order reaction kinetics for the prepared photocatalysts compared with the commercial TiO_2 (P25) film. The control experiments showed that there was no degradation of MB over the photocatalysts in the absence of UV light, indicating that the MB adsorption on the photocatalysts could be negligible. Furthermore, no degradation of MB was observed in the absence of photocatalysts. Under UV irradiation, a sudden decrease in the MB concentration occurred over the photocatalysts. In Fig. 4(a), the photocatalytic efficiency of nanorod film, nanodrop and commercial P25 films for MB degradation was about 94, 47 and 35%, respectively, after irradiation for 90 min. The specific surface area of the photocatalysts obtained from flat-shaped nozzle and wedge-shaped nozzle was 35.7 and 18.5 m^2/g, respectively. The TiO_2 nanorod film possessed the highest photocatalytic efficiency probably due to its higher surface area, resulting in more efficient contact of the photocatalyst with organic contaminants.

Fig. 4(b) shows a linear plot of $\ln(C/C_0)$ versus irradiation time for MB degradation over different catalysts. The MB photodegradation obeyed the pseudo first-order kinetics. The apparent rate constant (k_{app}) of the nanorod film, nanodrop film and commercial P25 film was 0.0307, 0.0072 and 0.0048 min^{-1}, respectively. The k_{app} value of TiO_2 nanorod film was about 4.3 times larger than that of nanodrop film and about 6.4 times larger than that of commercial P25 film. This might be because the TiO_2 nanorod film appears 3D nanostructure created from an interconnection of 1D structured TiO_2 nanorod, leading to the direct pathway for electron transportation from 1D structure [26] and light trapping by light multi-scattering [27], the decreased charge recombination rate and the increased separation of charge carriers, as shown in the EIS result.

The catalyst stability and reusability of the resulting photocatalyst film were also investigated. Therefore, the circulating runs for the photocatalytic degradation of MB were carried out. The catalyst film could repeatedly be used without any treatment and could easily be separated by simply taking the film out of the solution. The photocatalytic efficiency of the catalyst film did not show any noticeable loss even after five reuse cycles, as demonstrated in Fig. 5.

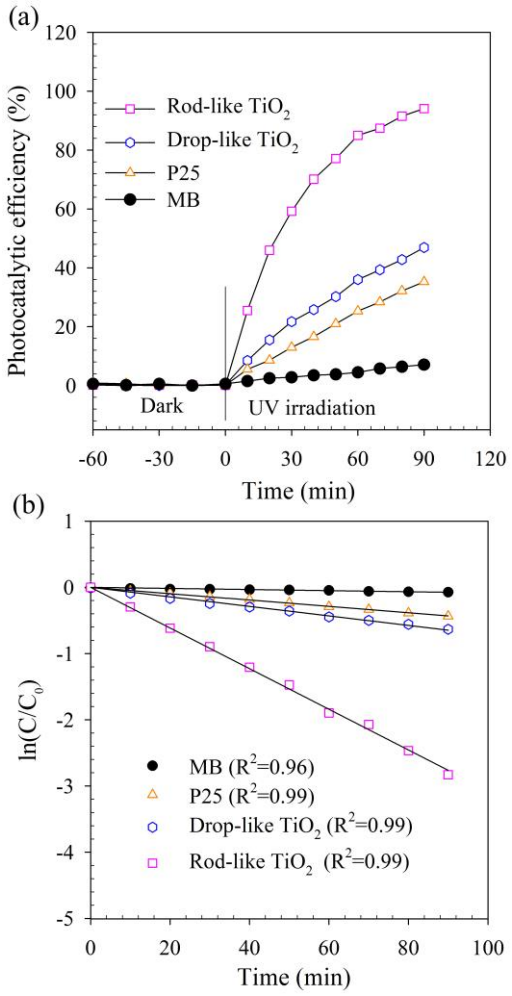

Fig. 4. (a) Photocatalytic efficiency for MB degradation under UV irradiation (with the time of light on set as 0) and (b) the plots of ln(C/C$_0$) versus reaction time

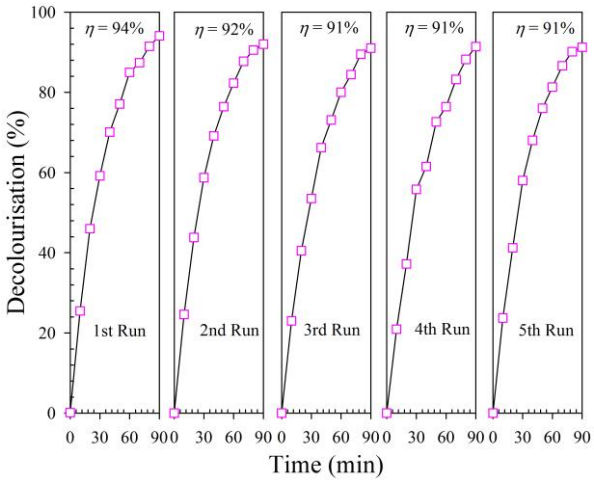

Fig. 5. Reusability of the rod-like TiO$_2$ film for five cycles

4. Conclusions

3D hierarchical nanostructured porous TiO_2 films with different morphologies were produced using ESD process. Rod- and drop-like architectures of TiO_2 films with anatase phase could be obtained by tuning the nozzle geometry. The use of the nozzle with flat-shaped tip (0°) gave rod-like film, whereas the use of that with wedge-shaped tip (15°) gave drop-like films. The photocatalytic efficiency of 3D hierarchical porous TiO_2 film with rod-like nanostructure for MB degradation was higher than that with drop-like nanostructure and P25 film obtained from commercial Degussa powder. The remarkable improvement in photocatalytic performance was attributed to the 3D rod-like network structure and the reusability observation also revealed that the photocatalyst film with high efficiency and stability could be used for practical application in wastewater treatment.

Acknowledgment

The authors are grateful for the financial support of Silpakorn University Fund for Research and Creative Work (Faculty of Engineering and Industrial Technology).

References

[1] J. Shi, C. Sun, M.B. Starr, X. Wang, Nano Lett. **11**, 624 (2011).
[2] H. B. Wu, H. H. Hng, X. W. Lou, Adv. Mater. **24**, 2567 (2012).
[3] T. Zhu, W. L. Ong, L. Zhu, G. W. Ho, Sci. Rep. **5**, 10601 (2015).
[4] M. Gao, L. Zhu, W. L. Ong, J. Wang, G. W. Ho, Catal. Sci. Technol. **5**, 4703 (2015).
[5] L. Mao, Y. Wang, Y. Zhong, J. Ning, Y. Hu, J. Mater. Chem. A. **1**, 8101 (2013).
[6] G. Tian, Y. Chen, W. Zhou, K. Pan, C. Tian, X.-r. Huang, H. Fu, Cryst Eng Comm. **13**, 2994 (2011).
[7] C. X. Wang, L. W. Yin, L. Y. Zhang, Y. X. Qi, N. Lun, N. N. Liu, Langmuir. **26**, 12841 (2010).
[8] A. Javey, S. Nam, R. S. Friedman, H. Yan, C. M. Lieber, Nano Lett. **7**(3), 773 (2007).
[9] H. W. Bai, Z. Y. Liu, S. S. Lee, D. D. Sun, Appl. Catal. A. **447–448**, 193 (2012).
[10] B. Ksapabutr, W. Thong-oun, M. Panapoy, Funct. Mater. Lett. **2**, 179 (2009).
[11] G. Poungchan, B. Ksapabutr, M. Panapoy, Mater. Des. **89**, 137 (2016).
[12] J. Wang, B. He, X. Z. Kong, Appl. Surf. Sci. **327**, 406 (2015).
[13] I. Chauhan, P. Mohanty, RSC Adv. **4**, 57885 (2014).
[14] N. M. Bedford, M. Pelaez, C. Han, D. D. Dionysiou, A. Steckl, J. Mater. Chem. **22**, 12666 (2012).
[15] H. Lee, M. Y. Song, J. Jurng, Y.-K. Park, Powder Technol. **214**, 64 (2011).
[16] R. S. Sonawane, S. G. Hegde, M. K. Dongare, Mater. Chem. Phys. **77**, 744 (2003).
[17] L. M. S. Colpini, G. G. Lenzi, M. B. Urio, D. M.

Kochepka, H. J. Alves, J. Environ. Chem. Eng. **2**, 2365 (2014).
[18] B. Ksapabutr, M. Panapoy, K. Choncharoen, S. Wongkasemjit, E. Traversa, Thin Solid Films. **516**, 5618 (2008).
[19] B. Ksapabutr, P. Nimnuan, M. Panapoy, Mater. Lett. **153**, 24 (2015).
[20] B. Ksapabutr, T. Chalermkiti, S. Wongkasemjit, M. Panapoy, Thin Solid Films. **546**, 423 (2013).
[21] R. Neagu, E. Djurado, L. Ortege, T. Pagnier, Solid State Ionics. **177**, 1443 (2006).
[22] N. Sangkharat, N. Chaiyut, B. Ksapabutr, M. Panapoy, Ceram. Int. **42**, 5858 (2016).
[23] W. Wei, Z. Gu, S. Wang, T. Fukuda, K. Kase, J. Ju, Y. Yamagata, Y. Tajima, Particuology. **11**, 20 (2013).
[24] Q. Xiao, O. Linli, Chem. Eng. J. **148**, 248 (2009).
[25] H. Cai, Q. Yang, Z. Hu, Z. Duan, Q. You, J. Sun, N. Xu, J. Wu, Appl. Phys. Lett. **104**, 053114 (2014).
[26] X. Wang, Z. Li, J. Shi, Y. Yu, Chem. Rev. **114**, 9346 (2014).
[27] C. Cheng, H. Zhang, W. Ren, W. Dong, Y. Sun, Nano Energy. **2**, 779 (2013).

*Corresponding authors: kbussarin@gmail.com, mpanapoy@hotmail.com